DOI: http://dx.doi.org/10.32571/ijct.1564244 **E-ISSN: 2602-277X**

International Journal of Chemistry and Technology

http://dergipark.org.tr/ijct

Research Article

In Vitro Assessment of Antiproliferative Properties of a Novel Benzoxazole-Conjugated Pyrrolotriazinone

Burak Kuzu[1], Kemal Alp Nalcı[2]*

[1]*Department of Pharmaceutical Chemistry, Faculty of Pharmacy, Van Yüzüncü Yıl University,65080, Van, Türkiye*

[*2]*Department of Pharmacology, Faculty of Pharmacy, Van Yüzüncü Yıl University,65080, Van, Türkiye*

Received: 10 October 2024; Revised: 4 January 2025; Accepted: 7 February 2025

*Corresponding author: kemalalpnalci@yyu.edu.tr

Citation: Kuzu, B.; Nalcı, K.A. *Int. J. Chem. Technol.* **2025**, 9(1), 107-116.

ABSTRACT

In this study, a new class of antiproliferative agents was designed and synthesized against glioblastoma, the most lethal and aggressive primary brain tumor. The structure was designed by hybridizing benzoxazole and pyrrolotriazinone, two important pharmacophore groups for antiproliferation. The target compound was synthesized in a six-step procedure. The structure of the benzoxazole-conjugated pyrrolotriazinone compound was characterized by FT-IR, ^{1}H- and ^{13}C-NMR spectra. It was found to have favorable drug similarity and theoretical pharmacokinetic parameters according to *in silico* methods. The antiproliferative effect of the target compound on the glioblastoma cell line U-87 MG was evaluated, showing dose-dependent effectiveness. Furthermore, this study investigates the molecular docking of the novel compound with key glioblastoma-associated targets, revealing its potential as a multi-target therapeutic agent. The compound demonstrates strong binding affinity and inhibitory potential against VEGFR-2, VEGFR-1, and PI3K, and shows significant activity in apoptotic pathways through Caspase-3 and BCL-2. These results suggest its potential to disrupt tumor growth, angiogenesis, and cell proliferation. Overall, the benzoxazole-conjugated pyrrolotriazinone hybrid structure shows promise for glioblastoma treatment and could represent a significant step forward in the design of new drug candidates in the future.

Keywords: Antiproliferation, benzoxazole, druglikeness, glioblastoma, pyrrolotriazinone.

1. INTRODUCTION

Cancer is a complex and serious disease characterized by the uncontrolled proliferation of tumor cells.[1] This abnormal growth allows cancer cells to exploit surrounding tissues and blood vessels, leading to metastasis the process by which cancer spreads to distant sites in the body.[2] Ultimately, these processes can lead to significant morbidity and mortality. Under normal physiological conditions, cellular homeostasis is maintained through a regulated cycle of cell growth, differentiation, and apoptosis, whereby damaged or unnecessary cells receive signals to undergo programmed cell death and are subsequently replaced by new, healthy cells.[3] In contrast, cancer cells evade these regulatory mechanisms and often exhibit features such as sustained proliferative signaling, resistance to cell death, and the ability to manipulate their microenvironment.[4] This manipulation may include secretion of growth factors, alteration of the extracellular matrix, and recruitment of immune cells that inadvertently support tumor growth.[5] Consequently, cancer cells can survive and inhibit the proliferation and function of neighboring healthy cells, contributing to a microenvironment that favors tumor progression.

As the disease progresses, it often reaches advanced stages where treatment options become more limited and less effective. The interplay between cancer cells and their microenvironment is a crucial area of research

DOI: http://dx.doi.org/10.32571/ijct.1564244 E-ISSN: 2602-277X

as understanding these dynamics can lead to the development of novel therapeutic strategies aimed at disrupting the mechanisms that allow tumors to thrive.[6] Today, many methods such as surgery, radiation therapy and chemotherapy can be used to slow the progression of cancer and improve the quality of life of cancer patients. However, the treatment methods mentioned usually do not provide a solution. Therefore, researchers are focusing on developing targeted cancer treatment methods, particularly studies of cancer treatment at the cellular level. Although chemotherapy drugs undoubtedly represent an important key point in the cellular treatment of cancer, the negative effects of these agents on healthy cells and drug resistance of cancer cells limit the use of chemotherapy drugs.[7] Studies are therefore still ongoing to develop chemotherapy drugs with a low side effect profile. Numerous studies have concluded that the development of new targeted chemotherapy drugs with fewer side effects is crucial for modern cancer treatment.[8]

Glioblastoma is the deadliest and most aggressive primary brain tumor.[9] Glioblastoma, which can also occur in the spinal cord, is a malignant brain tumor and has histological features such as enlargement of the blood vessels around the tumor and the development of necrosis.[10] Although surgical or chemotherapy interventions are possible in the advanced stages of glioblastoma diagnosis, unfortunately this only results in the patient living a few months longer. Treating glioblastoma with chemotherapy is more difficult because the drugs cannot cross the blood-brain barrier.[11] Therefore, the development of new chemotherapy drugs for the treatment of glioblastoma is a very important research topic.

There are several problems that need to be addressed currently in the used of drugs to treat glioblastoma, such as low selectivity, high toxicity, and drug resistance.[12] To overcome these problems, various natural and synthetic heterobicyclic compounds are being developed and their effects in cancer treatment are being studied. Among the heterobicyclic compounds, new synthetic compounds with hybrid systems of fused heterocyclic ring systems in particular show promising results in cancer treatment.[13]

Among heterocyclic compounds, benzoxazole and its isosteric structures can interact with nucleotides as they are biosteres of DNA and RNA nucleotides and represent an ideal scaffold for targeted activities.[14] In previous studies on the benzoxazole ring system, the anticancer activity potential of benzoxazole derivatives (**1**) obtained from natural sources was remarkable and enabled the preparation of synthetic derivatives (**2**) of these compounds. Among recently developed synthetic benzoxazole derivatives, carboxamide-substituted benzoxazole derivative compound **3** was observed to exhibit strong antiproliferation for MCF-7 cell line among various cancer cell lines and arrest cancer cells in G0/G1 phase.[15] The pyrrole-substituted benzoxazole derivative compound 4, developed based on this compound, was reported to induce apoptosis in MCF-7 cancer cells with an IC_{50} concentration of 4.29 µM (Figure 1).[16]

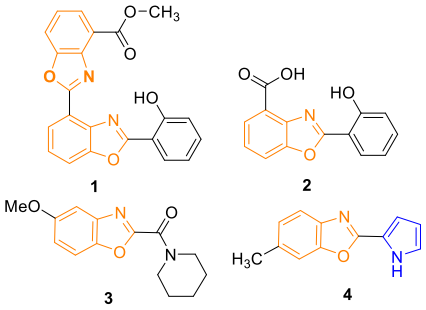

Figure 1. Some benzoxazole derivatives as antiproliferative agents.

It is observed that the antiproliferative effect increases with the substitution of the benzoxazole ring with the pyrrole system. Based on this, fused-pyrrole systems are also reported to be highly effective bioactive compounds in the literature.[17] Among the fused-pyrrole systems, interestingly, the limited availability of pyrrolotriazinone derivatives and the unique bioactivity potential exhibited by compounds with this structure make pyrrolotriazinone derivatives a scaffold waiting to be discovered.[18] For example, among pyrrolotriazinone derivatives, it was found that compound 5 derivatives had suitable druggability parameters, and compound 6 showed *in vitro* and *in vivo* activity by targeting Eg5 in the leukemia model (IC_{50}: 60 nM). In addition, compound 6 was found to have antiproliferative effect as a PI3Kγ−PI3Kδ dual inhibitor with very high potency and selectivity.[19,20] Pyrrolotriazinone derivatives, which were developed based on this structure and have been the subject of many patents, have also been identified as PI3K inhibitors (Figure 2).[21.]

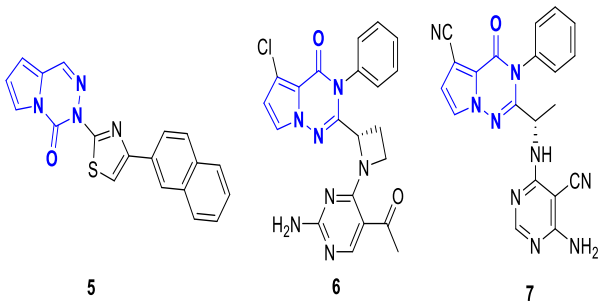

Figure 2. Pyrrolotriazinone derivatives with druggable and anticancer potential.

In this study, a new hybrid compound containing benzoxazole and pyrrolotriazinone structure from fused-heterocyclic systems was designed within the scope of all these data (**Figure 3**). The synthesized compound was purified by column chromatography while ^{1}H-NMR,

DOI: http://dx.doi.org/10.32571/ijct.1564244 E-ISSN: 2602-277X

^{13}C-NMR spectroscopy, and elemental analysis were used for structure characterization.

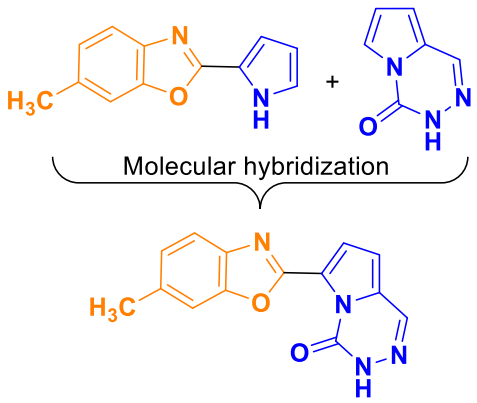

Figure 3. Designing potential derivatives against glioblastoma through molecular hybridization.

Furthermore, the antiproliferative effect of the produced compound on glioblastoma cancer cell line U-87 was investigated. Additionally, the drug-likeness and theoretical pharmacokinetic profiles of the compound were investigated, and the molecular docking studies revealed that the targeted compound exhibits a strong binding potential with several cancer-associated proteins.

2. EXPERIMENTAL

2.1. Materials

All solvents, reactants, and catalysts used in this study are of analytical purity. ^{1}H- and ^{13}C-NMR spectra were recorded on a Varian-Agilent Inova instrument (400 MHz) using Me_4Si as the internal standard. Melting points were determined on a Stuart Melting Point (SMP30) analyzer using open glass capillaries. Column chromatography was performed on silica gel (60 mesh, Silycycle). Commercially available materials were used without further purification. The analyses of the C, H, and N elements of the compounds were made with the LECO 932 CHNS (St. Joseph, MI, USA) elemental analysis device. Analysis results have a maximum deviation of ±0.4 from the calculated theoretical values. Fourier Transform Infrared (FTIR) spectroscopy, a technique used to identify the functional groups within a molecule's structure, was employed to characterize the compound. The analysis was conducted using an Agilent Cary 630 FT-IR spectrometer.

RPMI 1640 (Cat No: R8758), FBS (Fetal Bovine Serum, Cat No: F7524), PSA (Antibiotic Antimycotic Solution (100×), Stabilized Cat No: A5955), DPBS (Dulbecco's Phosphate Buffered Saline Cat No: D5773) were obtained from Sigma-Aldrich, MTT (Cat No: BD251612) provided by BLDpharm, Flasks and well plates (Product No:CLS431463 and P6991) gathered from Corning , Trypsin EDTA (Product No: T4049) gathered from Thermo Fisher, DMSO (Dimethyl sulfoxide, Cat No: A13280) obtained from Alfa Aesar.

2.2. Methods

2.2.1. Chemistry

Synthesis of 1*H*-pyrrole-2-carbaldehyde

10 mL DMF was taken into a flask and cooled in an ice bath. 10 mmol $POCl_3$ was added dropwise to the reaction flask and stirred at this temperature for 15 min. After the completion of the time, 5 mmol of commercially available pyrrole was added dropwise to the main reaction solution at 0°C. The reaction was left to stir overnight at room temperature. After the completion of the reaction, 50 ml of water was added to the main flask and neutralized with aqueous NaOH solution until pH: 8. The reaction mixture was extracted with ethyl acetate (3x30 ml), the organic phase was collected and dried over $MgSO_4$. The crude product was purified by column chromatography on silica gel using the appropriate mobile phase (n-hexane/ethylacetate:5/1).[19]

Synthesis of (E/Z)-2 (((1H-pyrrol-2-yl)methylene)amino-5-methylphenol

3 mmol pyrrole carbaldehyde was dissolved in 7 mL absolute ethanol. 5 ml ethanol-dissolved 5-methyl-2-aminophenol solution was added dropwise at room temperature. The reaction was stirred at room temperature for 4 hours and the conversion of the starting compound to product was checked by TLC. After the reaction was terminated, it was decanted into ice-water mixture, and the particles formed were filtered and left to dry in the open air.[16]

Synthesis of 6-methyl-2-(1H-pyrrol-2-yl)benzo[d]oxazole

The intermediate product (1 mmol) obtained in the previous step was dissolved in 5 ml of dimethylformamide (DMF) and 0.1 g of NaCN was added. The reaction mixture was stirred at room temperature in the open air for 1 h. The reaction mixture was transferred to an ice-water mixture when the starting material disappeared to obtain the residue. The resulting residue was filtered and washed with brine. The final product, which gave a blue spot on TLC, was purified by column chromatography 4:1 (n-hexane:ethyl acetate).[16]

Synthesis of 5-(6-methylbenzo[d]oxazol-2-yl)-1H-pyrrole-2-carbaldehyde

1 mmol of 6-methyl-2-(1H-pyrrol-2-yl)benzo[d]oxazole was dissolved in 4 ml of dry DMF and 1.2 mmol of phosphoryl chloride ($POCl_3$) was added. The reaction mixture was refluxed at 150°C for 4 h. After TLC

DOI: http://dx.doi.org/10.32571/ijct.1564244 E-ISSN: 2602-277X

control, the reaction was terminated, cooled to room temperature, and then neutralized with aqueous NaOH. The crude product was extracted with 3x20 ml of ethyl acetate and 50 ml of water and used for the next step without purification.

Synthesis of ethyl 2-formyl-5-(6-methylbenzo[d]oxazol-2-yl)-1*H*-pyrrole-1-carboxylate

1 mmol of the product obtained in the previous step was dissolved in 4 mL of DMF at 0°C and after 30 min, 1.8 mmol of NaH was added portionwise over 1 h. The resulting mixture was stirred for an additional 1 h at 0 °C and 1.2 mmol of ethyl chloroformate in 1 mL of DMF was added dropwise. The reaction mixture was stirred at room temperature for 2 h and after TLC control, the mixture was extracted with 3 × 20 ml of ethyl acetate and 50 ml of water. The extracts were washed with brine (2 × 15 ml), dried over $MgSO_4$ and evaporated. The crude product was purified by chromatography on silica gel, eluting with hexane-EtOAc, 5:1.[19]

Synthesis of the target compound

1.6 mmol of hydrazine hydrate (64%) was added to 10 mL of EtOH solution of the compound from the previous step. The reaction medium was refluxed for 90 min and after complete conversion of the starting compound to the product was observed, the reaction was terminated and cooled to room temperature. When 10 mL of water was added to the reaction mixture, a precipitate formed, and it was stirred at room temperature for 20 min. The solid particles formed in the medium were filtered and washed several times with 5 mL of cold EtOH and finally with 10 mL of water. The crude solid product was dried in the open air and then purified by chromatography on silica gel, eluting with hexane-EtOAc, 2:1.

6-(6-methylbenzo[d]oxazol-2-yl)pyrrolo[1,2-d][1,2,4]triazin-4(3H)-one

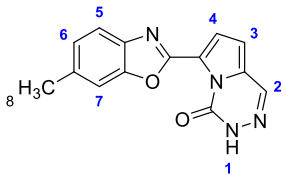

Yellow-orange powder, M.p.:206-207°C, Yield: 74%. ^{1}H NMR (400 MHz, d_6-DMSO) δ 12.86 (bs, 1H, -NH, H-1), 8.60 (bs, 1H, H-2), 7.59 (d, *J*= 8.1 Hz, 1H, H-5), 7.53 (d, *J*= 1.3 Hz, 1H, H-7), 7.20 (dd, *J*=1.3 Hz, *J*= 8.1 Hz, 1H, H-6), 7.06 (dd, *J*= 2.0 Hz, *J*= 3.9 Hz, 1H, H-4), 6.92 (dd, *J*= 2.0 Hz, *J*= 3.9 Hz, 1H, H-3), 2.45 (s, 3H, Ar-CH_3). ^{13}C NMR (100 MHz, d_6-DMSO) δ 156.6, 152.3, 150.4, 139.8, 135.5, 132.7, 126.4, 123.6, 123.1, 119.0, 114.7, 113.2, 111.1, 21.7. FT-IR (ATR cm^{-1}): 3276, 3029, 2918, 2847, 1718, 1657, 1602, 1457, 1132, 1017, 782. Anal. calcd. for $C_{14}H_{10}N_4O_2$: C: 63.15; H: 3.79; N: 21.04; Found: C: 63.11; H: 3.82; N: 20.98.

2.2.2. Pharmacokinetic calculations

The drug-likeness ADMET properties and the boiled-egg model of the compound were determined by online web tools. The SMILE of the compound was obtained from SwissADME (https:/www.swissadme.ch). The absorption, distribution, excretion, metabolism (CYP450 substrate or inhibitor), and toxicity parameters were evaluated by ADMETLab 2.0.[22]

2.2.3. Cancer Cell Culture and Cytotoxicity

To evaluate the anticancer activity of the synthesized molecule, the cell line U-87-MG was used. 10,000 cells were cultured per well. After waiting for one day and reaching 80% confluence, the determined doses of the molecule were applied (1666 micromolar- 20 micromolar). After applying the doses determined for the MTT test, the cell fluid was removed. MTT solution (%10 w/w) was added to the wells. After 4 hours of incubation in the dark, the supernatant was withdrawn and 100 microliters of DMSO was added and the optical densities were measured at an absorbance of 570 nm. The ratio was determined by assuming the viability of the control group to be 100%. The IC_{50} value of the molecule was determined using the GraphPadPrism 8.0 program and its graph was created.[23,24]

2.2.3. Statistical Analysis

Statistical analyses were performed using IBM SPSS 20.0 One-Way ANOVA Post-Hoc Duncan test. $p<0.05$ was accepted. Graphs were drawn with the GraphPad Prism 8.0 program.[25]

2.2.4. Molecular Docking Simulations

Molecular docking studies were conducted using AutoDock 4.2 software to identify the interactions of target compound against 3D structures of BCL-2, Caspase-3, VEGFR-1, VEGFR-2, and PI3K. The crystal structure of the BCL-2 (PDB ID: 4MAN), Caspase-3 (PDB ID: 5I9B), VEGFR-1 (PDB ID: 3HNG), VEGFR-2 (PDB ID: *4MAN*), and PI3K (PDB ID: 2XIR) were obtained from the RCSB Protein Data Bank (www.rcsb.org). The molecular structure of the target compound was drawn using Gaussview 5.0 and then optimized using the DFT method with the help of the Gaussian 03 package based on the theoretical level of the B3LYP method and the 6–31G basis set. Docking processes started with removing the unwanted solvent, water, and ligands from the crystal structures. In docking studies, for BCL-2 x: -12.621; y: 8.675; z: 7.516, for Caspase-3 x: -3.156; y: -13.42; z: -18.754, for VEGFR-1 x: 7.217; y: 21.488; z: 30.462, for VEGFR-2 x: 21.22; y: 25.101; z: 40.255 and for PI3K x: 37.261, y: 16.906, and z: 34.242 were determined as coordinate centers.[26] Then, using a grid box with 50×50×50 points

DOI: http://dx.doi.org/10.32571/ijct.1564244 E-ISSN: 2602-277X

at the center of the predicted locations and a grid point spacing of 0.375 Å, the lowest-placed conformations were selected for further studies. Water molecules were removed with AutoDock tools, and subsequently, polar hydrogen atoms, Gasteiger partial charges, and Kollman charges were added to the targets. Additionally, the rotatable bonds of the compounds were adjusted. The target regions of the selected compounds were docked under validated conditions using Autodock 4.2 software. To validate the docking process on the specified target, the native ligand was re-docked and overlapped with the experimentally solved crystal geometry. The Lamarckian genetic algorithm (10 runs) approach was applied, and the population size was set to 300 for both simulations. The interactions of crystal structures with the compound were analyzed using the Discovery Studio Client 4.1 program.

3. RESULTS and DISCUSSION

3.1. Chemistry

The synthetic approaches applied to obtain the target compound are presented in Figure 4. This method consists of six steps; initially, commercially available pyrrole is converted to pyrrole-carboxaldehyde derivative with Vilsmeier-Haack reagents ($POCl_3$, DMF). In the next step, the imine functional group is obtained by reaction of aldehyde group with 2-amino-5-methylphenol and then benzoxazole-2-pyrrole derivative is obtained under NaCN catalyst. The obtained compound is treated with Vilsmeier-Haack reagents again, this time resulting in carbaldehyde substitution at position 5 of pyrrole. Then, the main reagent for the synthesis of the target compound is formed by substituting pyrrole with ethylformate. In the last step, the targeted Benzoxazole-Conjugated Pyrrolotriazinone structure is synthesized after reaction of the main reagent with hydrazine hydrate.

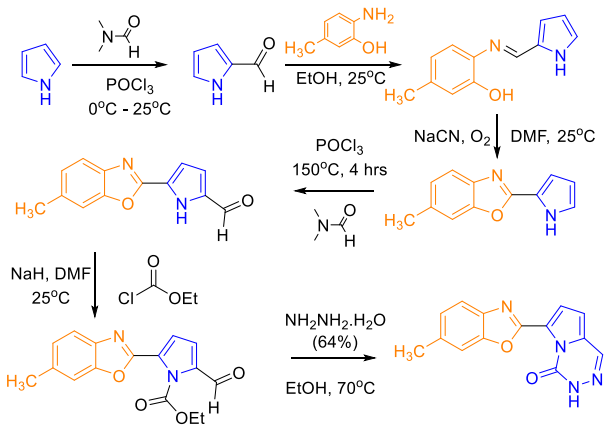

Figure 4. Total synthesis scheme of the target compound.

NMR analysis data supported the success of the applied route. The ^{1}H-NMR spectrum of the compound revealed that the -NH group in the triazole ring resonated as a broad singlet at 12.86 ppm, and the characteristic -HC=N (position 2) group in the triazinone ring resonated as a broad singlet at 8.60 ppm, interacting with the protons of the pyrrole ring. The doublet peak (J=8.1 Hz) observed at 7.59 ppm belongs to the aromatic hydrogen (position 5) in the *ortho* position of the benzoxazole ring. The protons of the benzoxazole ring resonate as follows: The proton at position 7 appears as a doublet at 7.53 ppm, coupled with the proton at position 6, exhibiting a coupling constant of J = 1.3 Hz. The proton at position 6 resonates at 7.20 ppm as a doublet of doublets (dd), influenced by both the proton at position 7 (J = 1.3 Hz) and the proton at position 5 (J = 8.1 Hz). Finally, the protons at positions 4 and 3 of the pyrrole ring resonated at 7.06 and 6.92 ppm, respectively, as a doublet of doublet (J= 2.0 Hz and J= 3.9 Hz) because they interacted with each other and the -HC=N proton (position 2) on the triazinone ring. Additionally, the aryl-CH_3 group of the benzoxazole ring resonated in the range of 2.45 ppm. It was observed that all other aromatic protons in the compounds were as expected in the ^{1}H-NMR spectrum (Figure 5), and all ^{13}C-NMR spectrum (Figure 6) signals also matched the type and number of carbons in the compounds.

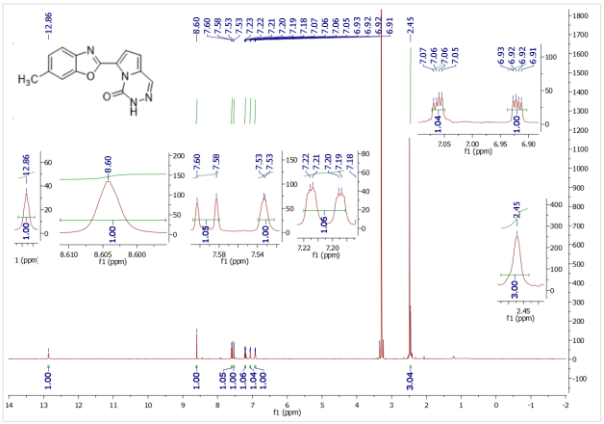

Figure 5. ^{1}H-NMR spectrum of the target compound

DOI: http://dx.doi.org/10.32571/ijct.1564244 E-ISSN: 2602-277X

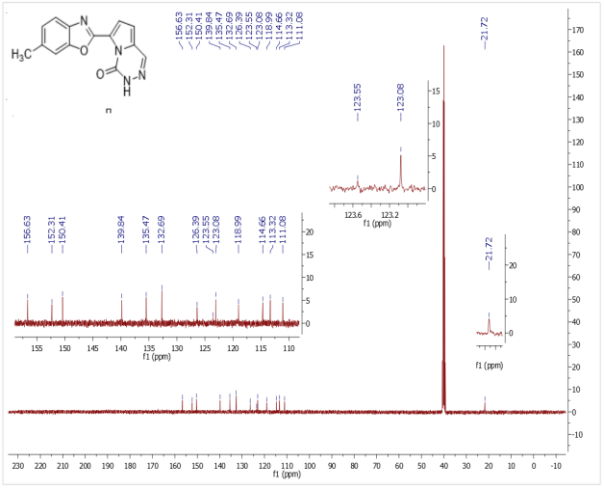

Figure 6. ^{13}C-NMR spectrum of the target compound.

The FT-IR (ATR) spectrum of the target compound provides valuable insights into the functional groups and molecular structure of the compound (Figure 7). The broad band observed at 3276 cm^{-1} is attributed to the presence of an N-H group, indicating potential hydrogen bonding interactions. The peak at 3029 cm^{-1} corresponds to aromatic C-H stretching vibrations, which are characteristic of the aromatic rings in the structure. C-H stretching bands for the methyl groups are observed at 2918 cm^{-1} and 2847 cm^{-1}, confirming the presence of methyl groups in the molecule. The strong absorption at 1718 cm^{-1} and the weaker band at 1657 cm^{-1} are indicative of the C=O (carbonyl) stretching vibrations, which correspond to the carbonyl group in the triazine moiety. Additionally, the peak at 1602 cm^{-1} is attributed to the aromatic C=C stretching, further confirming the presence of the benzo[*d*]oxazol ring in the structure. The bands observed at 1132 cm^{-1} and 1017 cm^{-1} are assigned to C-N stretching vibrations, which are typical of the nitrogen-containing bonds in both the triazine and benzo[d]oxazol rings. The band at 1457 cm^{-1} represents the alkyl bending vibrations, while the absorption at 782 cm^{-1} is related to aromatic C-H out-of-plane bending vibrations. Overall, the FT-IR spectrum provides a clear identification of the key functional groups and structural features of the compound, including aromatic rings, methyl groups, carbonyl, and nitrogen-containing bonds. These observations are consistent with the proposed molecular structure and confirm the presence of the expected functional groups.

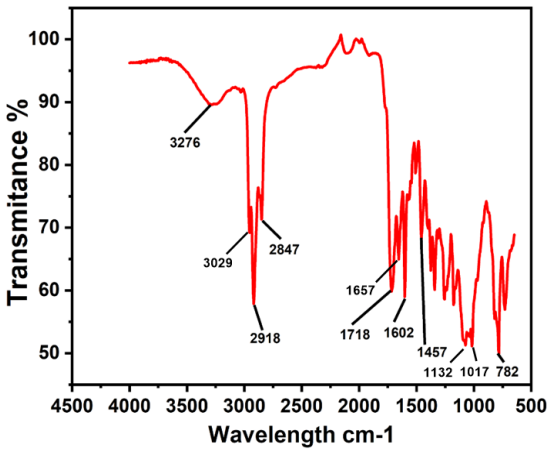

Figure 7. FT-IR spectrum of the target compound.

3.2.The Drug-likeness and Theoretical Pharmacokinetic Profiles

New drug candidate compounds need to have acceptable drug similarity and pharmacokinetic properties for clinical stages. Determining these properties in advance allows for a more rational design of drug candidates. Therefore, we investigated some drug similarity parameters of the target compound and found that the compounds obey Lipinski, Pfizer and GSK rules, which are acceptable according to their physicochemical properties. We performed a comprehensive analysis of drug similarity and key pharmacokinetic parameters associated with the target compound, which are detailed in Table 1.

Among the pharmacokinetic parameters, Caco-2 permeability is an *in vitro* model used for the passage of orally administered drugs through the human intestinal mucosa. The Caco-2 permeability of the compound was estimated as 0.876 10^{-6} cm/s and the estimated human intestinal absorption percentage (98.142%) was found to be quite high. The measure of the ability of the drug to distribute at the same concentration in the blood plasma after absorption is usually determined by the steady-state volume of distribution (VDss), this value is desired to be higher than 0.45 L/Kg and this value was found to be quite satisfactory as 0.669 L/Kg for the compound.

In addition, one of the most basic properties that a drug candidate designed for glioblastoma should have is the ability to cross the blood-brain barrier. The blood-brain barrier (BBB) value of the candidate compound was found to be -1.103 logBB and it was seen that it crossed the blood-brain barrier compared to the yolk of a BOILED egg. In addition, it was found that the compound was not a substrate for any of the cytochrome P-450 enzymes but was only an inhibitor of CYP1A2 and CYP2C8. It can be concluded that more suitable drug candidates can be reached with various modifications that can be made on the compound. The CLplasma value of the synthesized molecules is

DOI: http://dx.doi.org/10.32571/ijct.1564244 E-ISSN: 2602-277X

estimated to be 4.29 ml/min/kg; this value is understood to be ideal if it is less than 5. In addition, since inhibition of hERG channels will cause long QT syndrome, it is desired that the candidate compound is not a hERG blocker. While this value, which is theoretically calculated and is in the range of 0-1, is desired to be close to 0 for the candidate compound, a value of 0.096 is highly desired for the target compound. Another important parameter for drugs is the AMES Toxicity, a short-term bacterial test used to identify carcinogens. This value is expected to be between 0 and 1, and values greater than 1 indicate the possibility of the chemical being carcinogenic. The target compound has a value of 0.393 that falls within this range and has an acceptable AMES Toxicity profile.

Table 1. Some drug-likeness and ADMET Parameters.

Drug-likeness profiles				Pharmacokinetic properties			
Mw	266.25	**TPSA**	76.19	**Caco-2 permeability, (10^{-6} cm/s)**	0.876	**CYP substrate or inhibitor***	CYP1A2* CYP2C8*
LogP	2.627	**Lipinski Rule**	Accepted	**Intestinal absorption (%)**	98.142	**CL_{plasma} ml/min/kg**	4.29
HBA	4	**Pfizer Rule**	Accepted	**VDss (L/kg)**	0.669	**hERG Blockers**	0.096
HBD	1	**GSK Rule**	Accepted	**BBB permeant (Log BB)**	-1.103	**AMES Toxicity**	0.393

Furthermore, the BOILED-EGG model is an *in silico* tool used to predict key pharmacokinetic properties of drug candidates, such as their ability to cross the blood-brain barrier (BBB) and their intestinal absorption (HIA). This model is particularly useful in the early stages of drug development as it provides a rapid, cost-effective method for evaluating compounds without the need for extensive experimental studies.[27]

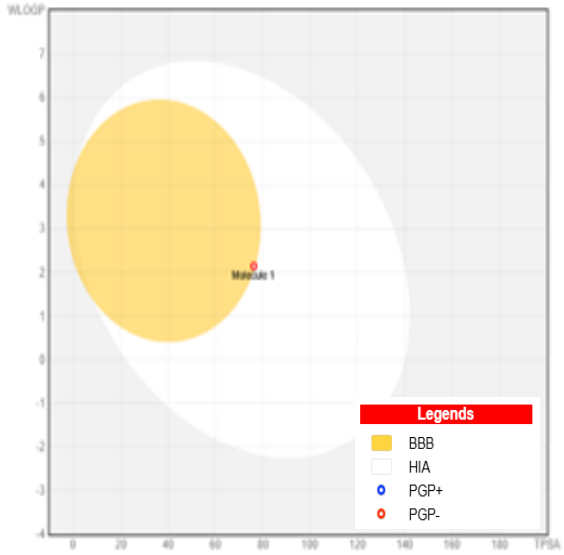

Figure 7. The boiled-egg model of the target compound.

The model classifies compounds based on their lipophilicity and hydrophilicity, which are essential factors for determining their bioavailability. The visual representation in the form of an "egg" allows researchers to see whether a compound is likely to penetrate the BBB or be absorbed by the intestines, both of which are crucial for drug efficacy. Compounds that fall within certain "ideal" regions of the model are considered more likely to exhibit favorable pharmacokinetic properties, while those outside these areas may face challenges related to absorption or BBB permeability. The BOILED-EGG model of the target compound is presented in Figure 7.

Analysis of the target compound using the boiled egg model indicates that it occupies a favorable position in terms of gastrointestinal bioavailability. However, its limited potential to cross the blood-brain barrier (BBB) represents a significant limitation for therapeutics targeting glioblastoma and other central nervous system (CNS) disorders. The molecule's TPSA (Topological Polar Surface Area) and WLOGP (lipophilicity indicator) values suggest a balanced pharmacokinetic profile. Nevertheless, optimizing these parameters, such as reducing TPSA or increasing lipophilicity, could enhance brain penetration, making the compound more effective for CNS-targeted therapies.

This molecule serves as an important starting point for the development of more effective therapeutics against glioblastoma. The pharmacokinetic properties of the target compound demonstrate a robust foundation for addressing the challenges posed by this difficult target. However, its limited ability to cross the BBB highlights the need for structural optimization. Strategies to lower the TPSA value or increase lipophilicity should be

DOI: http://dx.doi.org/10.32571/ijct.1564244 E-ISSN: 2602-277X

considered to improve BBB permeability. Such optimization efforts could significantly enhance the therapeutic potential of the molecule, paving the way for the development of a more successful candidate for glioblastoma treatment.

3.3. Cell Viability Assay

Our newly synthesized benzoxazole-conjugated pyrrolotriazinone was investigated for their cytotoxic potential against human glioblastoma cancer U-87 MG cell line. Compared to the control group, a mortality of 56% was observed at the dose concentration of 1660 µM. At a dose concentration of 555 µM, 21% deaths were observed, at a dose of 185 µM 15%, at a dose of 61 µM 13% and at a dose of 20 µM 11%. When statistically evaluated, all administered doses are significant compared to the control group ($p = 0.001$). The IC_{50} value calculated for target compound was found to be 1112 µM Figure 8.

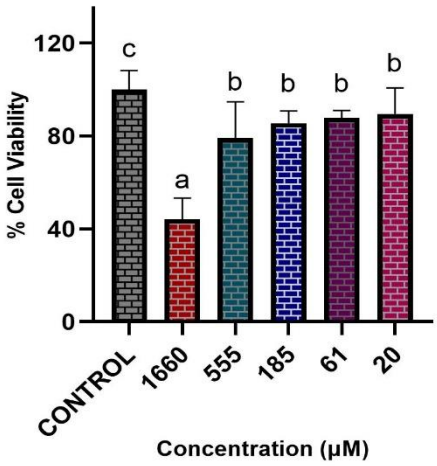

*Comparison of groups denoted by different letters with each other is statistically significant ($p<0.05$)

Figure 8. Cell viability of the target compound on the U-87 MG glioblastoma cancer cell line.

3.4. Molecular Docking Studies

The molecular docking results revealed the compound's interactions with five key glioblastoma-associated targets, highlighting its potential as a multi-target therapeutic agent Table 2.

Table 2. Docking scores of synthesized compounds against the target structures .

Targets	Binding affinity (kcal/mol)	Cluster RMSD (Å)	Inhibition Cons. (µM)
BCL-2	-6.94	0.10	8.21
Caspase-3	-7.49	0.30	3.23
VEGFR-1	-8.59	0.03	0.51
VEGFR-2	-8.96	0.02	0.27
PI3K	-8.06	0.04	1.23

Among the targets, the strongest binding affinity and inhibitory potential are observed for VEGFR-2 (binding affinity: -8.96 kcal/mol; IC_{50}: 0.27 µM), followed closely by VEGFR-1 (binding affinity: -8.59 kcal/mol; IC_{50}: 0.51 µM). Both receptors play critical roles in angiogenesis, and the compound's exceptional activity against VEGFR-2 makes it a particularly promising primary target for disrupting tumor vascularization and growth. The compound also demonstrates significant activity against PI3K, a key component of the PI3K/AKT/mTOR signaling pathway, with a binding affinity of -8.06 kcal/mol and IC_{50} of 1.23 µM. This suggests its potential to inhibit tumor proliferation and survival through the modulation of this frequently dysregulated pathway in glioblastoma. In terms of apoptotic pathways, the compound exhibits moderate activity against BCL-2 (binding affinity: -6.94 kcal/mol; IC_{50}: 8.21 µM) and stronger interaction with Caspase-3 (binding affinity: -7.49 kcal/mol; IC_{50}: 3.23 µM). While the activity against BCL-2 indicates some potential to disrupt anti-apoptotic mechanisms, the higher binding affinity and lower IC_{50} for Caspase-3 suggest a more effective role in activating apoptotic pathways in glioblastoma cells.

The docking results highlight VEGFR-2 as the most promising target for this compound, given its highest binding affinity (-8.96 kcal/mol) and lowest IC_{50} (0.27 µM). The 3D and 2D interaction images of the compound with the VEGFR-2 active site are presented in Figure 9 and Figure 10.

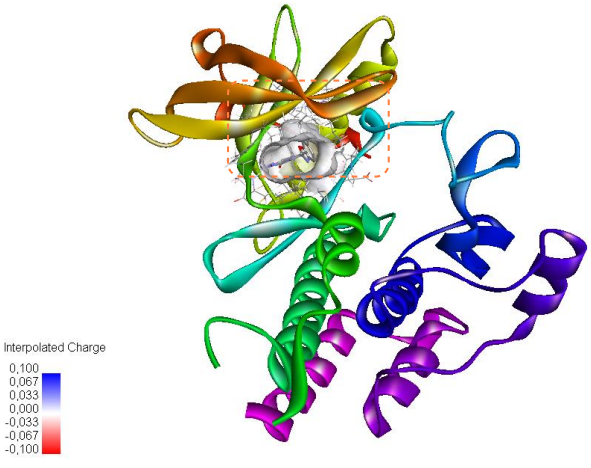

Figure 9. 3D ligand-protein interactions of VEGFR-2 active site with target compound.

DOI: http://dx.doi.org/10.32571/ijct.1564244 E-ISSN: 2602-277X

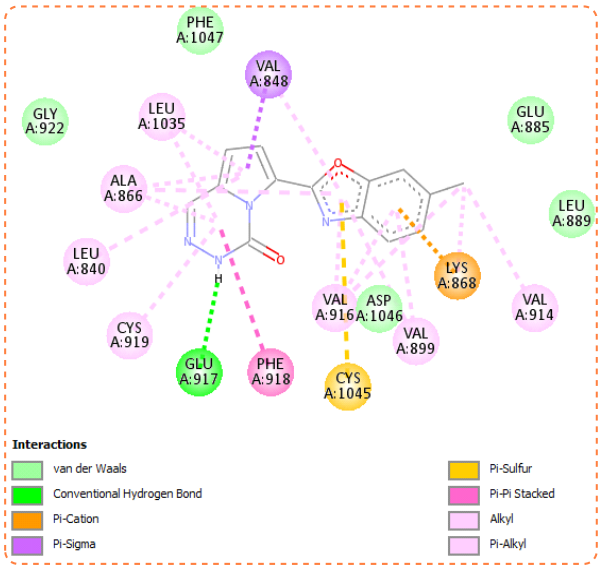

Figure 10. 2D ligand-protein interactions of VEGFR-2 active site with target compound.

The compound also demonstrates strong activity against) VEGFR-1, indicating its potential as an anti-angiogenic agent. Additionally, its interactions with Caspase-3 and PI3K suggest it could simultaneously induce apoptosis and inhibit tumor cell signaling pathways. However, its relatively moderate activity against BCL-2 indicates that further optimization may be needed to improve its pro-apoptotic effects.
These findings suggest that the molecule has the potential to act as a multi-target therapeutic agent for glioblastoma, combining anti-angiogenic, apoptotic, and anti-proliferative mechanisms.

4. CONCLUSION

A hybrid compound was synthesized incorporating benzoxazole and pyrrolotriazinone pharmacophores, both of which exhibit notable antiproliferative activity across diverse cancer cell lines. The target compound was successfully synthesized through a six-step process, and its molecular structure was characterized using spectral analysis techniques. Evaluation of the compound indicated an appropriate drug-like profile and favorable theoretical pharmacokinetic properties. *In vitro* assessments revealed that the compound displayed a dose-dependent antiproliferative effect against the U-87 MG glioblastoma cell line. The molecular docking results reveal the compound's interactions with five key glioblastoma-associated targets, highlighting its potential as a multi-target therapeutic agent. The docking scores for these targets showed strong binding affinity and inhibitory potential, particularly against VEGFR-2 (binding affinity: -8.96 kcal/mol; IC_{50}: 0.27 µM) and VEGFR-1 (binding affinity: -8.59 kcal/mol; IC_{50}: 0.51 µM), both of which play critical roles in angiogenesis. The compound's exceptional activity against VEGFR-2 makes it a promising primary target for disrupting tumor vascularization and growth.
The findings presented in this study suggest that the compound may serve as a foundational template for the development of more potent drug candidates for glioblastoma through subsequent molecular modifications.

Conflict of Interest

The authors declare no conflicts of interest.

REFERENCES

1. Bisoyi, P. A brief tour guide to cancer disease. Understanding Cancer; Jain, B., Pandey S., Eds.; Academic Press: **2022**, pp 1-20.
2. Zeeshan, R.; Mutahir, Z. Bosnian J. Basic Med. Sci. **2017**, 17(3), 172-182.
3. Kari, S.; Subramanian, K.; Altomonte, I. A.; Murugesan, A.; Yli-Harja, O.; Kandhavelu, M. Apoptosis **2022**, 27 (7), 482–508.
4. Morana, O.; Wood, W.; Gregory, C. D. Int. J. Mol. Sci. **2022**, 23 (3), 1328.
5. Quail, D. F.; Joyce, J. A. Nat. Med. **2013**, 19 (11), 1423–1437.
6. Guo, X.; Song, J.; Liu, M.; Ou, X.; Guo, Y. Cancer Biol. Ther. **2024**, 25 (1), 2356831.
7. Wang, X.; Zhang, H.; Chen, X. Cancer Drug Resist. **2019**, 2 (2), 141.
8. Anand, U.; Dey, A.; Chandel, A. K. S.; Sanyal, R.; Mishra, A.; Pandey, D. K.; de la Lastra, J. M. P. Genes Dis. **2023**, 10 (4), 1367–1401.
9. Lah, T. T.; Novak, M.; Breznik, B. In Seminars in Cancer Biology; Academic Press: **2020**; Vol. 60, pp 262–273.
10. D'Alessio, A.; Proietti, G.; Sica, G.; Scicchitano, B. M. Cancers **2019**, 11 (4), 469.
11. Wang, D.; Wang, C.; Wang, L.; Chen, Y. Drug Deliv. **2019**, 26 (1), 551–565.
12. Noch, E. K.; Ramakrishna, R.; Magge, R. World Neurosurg. **2018**, 116, 505–517.
13. Singh, S.; Utreja, D.; Kumar, V. Med. Chem. Res. **2022**, 1–25.
14. Kuzu, B.; Acikgoz, E.; Cakir, M. J. Mol. Struct. **2024**, 1309, 138199.

DOI: http://dx.doi.org/10.32571/ijct.1564244 **E-ISSN: 2602-277X**

15. Kuzu, B.; Hepokur, C.; Alagoz, M. A.; Burmaoglu, S.; Algul, O. ChemistrySelect **2022**, 7 (1), e202103559.

16. Kuzu, B.; Hepokur, C.; Turkmenoglu, B.; Burmaoglu, S.; Algul, O. Future Med. Chem. **2022**, 14 (14), 1027–1048.

17. Amărandi, R. M.; Al-Matarneh, M. C.; Popovici, L.; Ciobanu, C. I.; Neamțu, A.; Mangalagiu, I. I.; Danac, R. Pharmaceuticals **2023**, 16 (6), 865.

18. Ge, T.; Cintrat, J. C. Pharmaceuticals **2021**, 14 (12), 1275.

19. Kuzu, E.; Kuzu, B. Chem. Heterocycl. Compd. **2023**, 59 (1), 80–87.

20. Jia, H.; Dai, G.; Su, W.; Xiao, K.; Weng, J.; Zhang, Z.; Bembenek, S. D. J. Med. Chem. **2019**, 62 (10), 4936–4948.

21. Carrera Carrera, F.; Perez Garcia, J. B.; Vidal Juan, B.; Sanchez Izquierdo, F.; Serra Coma, M. C. WO Patent WO2015181052 A, **2015**.

22. Sicak, Y. Turk. J. Chem. **2022**, 46 (3), 665-676.

23. Özgür, G. K.; Dervişoğlu, G.; Özdemir, F. A.; Özdemir, N.; Şerbetçi, Z.; Dayan, O. Appl. Organomet. Chem. **2024**, 38 (2), e7342.

24. Çelik, Ş.; Dervişoğlu, G.; İzol, E.; Sęczyk, Ł.; Özdemir, F. A.; Yilmaz, M. E.; Khan, M. A. . Biomed. Chromatogr. **2024**, e5975.

25. Thornton, A. M.; Humphrey, R. M.; Kerr, D. M.; Finn, D. P.; Roche, M. Molecules **2021**, 26 (12), 3720.

26. Kuzu, B.; Arzuk, E. Chem. Biodiversity **2024**, e202401673.

27. Sıcak, Y.; Başaran, E.; Türkmenoğlu, B.; Öztürk, M. J. Mol. Struct. **2025**, 140417.